

# Electron correlation and spin-orbit coupling effects in $\text{US}_3$ and $\text{USe}_3$

Yu Yang<sup>1</sup> and Ping Zhang<sup>1,2,\*</sup>

<sup>1</sup>*LCP, Institute of Applied Physics and Computational Mathematics,  
P.O. Box 8009, Beijing 100088, People's Republic of China*

<sup>2</sup>*Center for Applied Physics and Technology,  
Peking University, Beijing 100871, People's Republic of China*

(Dated: August 23, 2018)

## Abstract

A systematic density functional theory (DFT) + $U$  study is conducted to investigate the electron correlation and spin-orbit coupling (SOC) effects in  $\text{US}_3$  and  $\text{USe}_3$ . Our calculations reveal that inclusion of the  $U$  term is essential to get energy band gaps for them, indicating the strong correlation effects for uranium  $5f$  electrons. Taking consideration of the SOC effect results in small reduction on the electronic band gaps of  $\text{US}_3$  and  $\text{USe}_3$ , but largely changes the energy band shapes around the Fermi energy. As a result,  $\text{US}_3$  has a direct band gap while  $\text{USe}_3$  has an indirect one. Our calculations predict that both  $\text{US}_3$  and  $\text{USe}_3$  are antiferromagnetic insulators, in agreement with corresponding experimental results. Based on our DFT+ $U$  calculations, we systematically present the ground-state electronic, mechanical and Raman properties for  $\text{US}_3$  and  $\text{USe}_3$ .

## I. INTRODUCTION

Actinide based materials possess interesting physical behaviors due to the existence of strongly-correlated  $5f$  electrons and have attracted extensive attentions<sup>1-6</sup>. Different from actinide oxides which have been widely studied to reveal the detailed configurations and correlation effects of the  $5f$  electrons<sup>5-30</sup>, none of the actinide chalcogenides has ever received comparable concerns. Here we take  $\text{US}_3$  and  $\text{USe}_3$  as two representatives to study the electron correlation and spin-orbit coupling (SOC) effects of  $5f$  electrons in actinide chalcogenides. The other reason for us to investigate their electronic structures is that they employ the layered  $\text{MX}_3$  structure (with M to be a metal element, and X to be S, Se, or Te), which can be used as models for studying electronic behaviors in 1-dimensional (1D) systems. The  $\text{MX}_3$  structure belongs to the space group of  $\text{P2}_1/m$ , with its atomic organizations depicted in Fig. 1(a). In the monoclinic lattice, the top two chalcogen (S, Se or Te) atoms form a tightly bound pair suggesting that the  $\text{MX}_3$  compounds may be regarded as  $\text{MX}(\text{X}_2)$ <sup>31</sup>. The top X-X pair together with an underneath M and a more underneath X atom form a triangular unit, which repeats along the  $\vec{b}$  lattice direction forming a 1D chain, and two such triangle units form a unit cell of the  $\text{MX}_3$  compounds in the  $(\vec{a}, \vec{c})$  plane. In this way, the  $\text{MX}_3$  compounds are always considered as 1D materials. For example, the metallic  $\text{ZrTe}_3$  and  $\text{NbSe}_3$  exhibiting charge-density-wave transitions have been thoroughly investigated in angle-resolved photoelectron spectroscopy (ARPES) and optical experiments<sup>32-36</sup>. In the present paper, by contrast, we address the electronic structures of  $\text{US}_3$  and  $\text{USe}_3$ , two semiconducting members of the  $\text{MX}_3$  family.

In studies of actinide based materials, one has to be careful for the electron correlation and SOC effects of the actinide  $5f$  electrons. As an example, for actinide dioxides conventional density functional theory (DFT) schemes that apply the local density approximation (LDA) or the generalized gradient approximation (GGA) underestimate the strong on-site Coulomb repulsion of the  $5f$  electrons and consequently fail to capture the insulating properties<sup>7,14</sup>. Several approaches, the LDA/GGA+ $U$ , the hybrid density functional of (Heyd, Scuseria, and Enzerhof) HSE, the self-interaction corrected local spin-density (SIC-LSD), and the Dynamical Mean-Field Theory (DMFT), have been developed to correct the pure LDA/GGA failures in calculations of actinide materials. Among them the effective modification of pure DFT by LDA/GGA+ $U$  formalisms has been widely used in theoretical studies of  $\text{UO}_2$ <sup>7,9,23</sup>

and  $\text{PuO}_2$ <sup>10–12,20</sup>. The obtained structural parameters as well as the electronic structure and phonon dispersion curves<sup>14,30</sup> accord well with experiments. In our present work, the GGA+ $U$  schemes due to Dudarev *et al.*<sup>7–9</sup> are employed to study the electron correlation and spin-orbit coupling effects in  $\text{US}_3$  and  $\text{USe}_3$ , as well as the two materials' electronic, mechanical, and Raman properties.

The rest of the paper is organized as follows. In Sec. II the computational method is briefly described. In Sec. III we present the results of the physical properties of  $\text{US}_3$  and  $\text{USe}_3$ , and discuss the electron correlation and SOC effects of the uranium  $5f$  electrons. Finally in Sec. IV, we close our paper with a summary of our main results.

## II. CALCULATION METHOD

Our total-energy calculations are carried out by employing the plane-wave basis pseudopotential method as implemented in Vienna ab initio simulation package (VASP)<sup>37</sup>. The exchange and correlation effects are described with the GGA approximation in the Perdew-Burke-Ernzerhof (PBE) form<sup>38,39</sup>. The projected augmented wave (PAW) method of Blöchl<sup>40</sup> is employed with the frozen-core approximation. Electron wave function is expanded in plane waves up to a cutoff energy of 400 eV and all atoms are fully relaxed until the Hellmann-Feynman forces on them are less than 0.01 eV/Å. A  $7 \times 9 \times 1$  Monkhorst-Pack<sup>41</sup> k-point mesh is employed for integration over the Brillouin zone of  $\text{US}_3$  and  $\text{USe}_3$ . The uranium  $6s^2 6p^6 5f^3 6d^1 7s^2$ , sulphur  $3s^2 3p^6$ , and selenium  $4s^2 4p^6$  electrons are treated as valence electrons. Noncollinear calculations are used when considering the spin-orbital coupling effects. The strong on-site Coulomb repulsions among the localized uranium  $5f$  electrons are described by using the formalism formulated by Dudarev *et al.*<sup>7–9</sup>. In this scheme, the total GGA energy functional is of the form

$$E_{\text{GGA}+U} = E_{\text{GGA}} + \frac{U - J}{2} \sum_{\sigma} [\text{Tr} \rho^{\sigma} - \text{Tr}(\rho^{\sigma} \rho^{\sigma})], \quad (1)$$

where  $\rho^{\sigma}$  is the density matrix of  $f$  states with spin  $\sigma$ , while  $U$  and  $J$  are the spherically averaged screened Coulomb energy and the exchange energy, respectively.

In this paper, the Coulomb  $U$  is treated as a variable, while the exchange energy is set to be a constant  $J=0.51$  eV. This value of  $J$  is in the ball park of the commonly accepted one for uranium compounds<sup>23</sup> and close to the theoretically predicted value of 0.54 eV in

UO<sub>2</sub><sup>42</sup>. Since only the difference between  $U$  and  $J$  is significant, we will henceforth label them as one single parameter  $U_{\text{eff}}=U-J$ , while keeping in mind that the nonzero  $J$  has been used during calculations.

The phonon frequencies at the Gamma point for US<sub>3</sub> and USe<sub>3</sub> are calculated by using the density functional perturbation theory (DFPT). And their Raman-active frequencies are obtained through symmetry analysis on the corresponding vibration modes. Before DFPT calculations, the lattice constants and atomic positions of US<sub>3</sub> and USe<sub>3</sub> are further optimized using a denser  $k$ -point mesh of  $9 \times 13 \times 3$ , and a finer force convergence criteria of 0.001 eV/Å. A  $2 \times 2 \times 1$  supercell is subsequently used for DFPT calculations. Since both US<sub>3</sub> and USe<sub>3</sub> are stacked along the  $\vec{c}$  direction through van der Waals interactions, and with relatively large lattice constants, we do not extend the supercell along the  $\vec{c}$  direction. During DFPT calculations on the  $2 \times 2 \times 1$  supercell, the  $k$ -point mesh is set to be  $5 \times 7 \times 5$ , and the energy convergence criteria is set to be 1e-6 eV.

### III. RESULTS AND DISCUSSION

Experimentally, the magnetic orderings of uranium trichalcogenides were studied ever since 1961<sup>31,43–46</sup>. The relatively large atomic distances between neighboring U atoms in US<sub>3</sub> and USe<sub>3</sub> suggest that magnetic orderings may occur in these compounds through super-exchange interactions of uranium 5*f* electrons via the S or Se ions<sup>31</sup>. And different measurements indicate that both US<sub>3</sub> and USe<sub>3</sub> crystals undergo AFM transitions at very low temperatures, with the magnetic moments of the two uranium atoms within each unit cell opposite to each other<sup>31,45,46</sup>. In the present GGA+ $U$  study, we consider the nonmagnetic (NM), ferromagnetic (FM), and antiferromagnetic (AFM) phases for each choice of the  $U_{\text{eff}}$  value and then determine the lowest-energy state by a subsequent total-energy comparison of these three phases. Our calculated electronic energies for different magnetic phases of US<sub>3</sub> and USe<sub>3</sub> are all listed in Table I. One can see that within GGA formalism or the GGA+ $U$  formalism with a too small  $U_{\text{eff}}$  value, the FM state is more stable for both US<sub>3</sub> and USe<sub>3</sub>, in contradiction with experimental results. Therefore, the electron correlation effect has to be accounted for to correctly describe ground-state US<sub>3</sub> and USe<sub>3</sub>. In the discussions that follow, we will confine our reports to the AFM solutions for US<sub>3</sub> and USe<sub>3</sub>.

The experimentally determined lattice parameters of US<sub>3</sub> and USe<sub>3</sub> are ( $a=5.37$  Å,  $b=3.96$

( $a=5.65$  Å,  $b=4.06$  Å,  $c=10.47$  Å) respectively<sup>31,47,48</sup>. Our calculated lattice constants with different  $U_{\text{eff}}$  values are summarized in Table II, together with the experimental results. We can see that different from what we found for actinide dioxides<sup>14,49</sup>, the lattice constants of actinide trichalcogenides do not change monotonically with the value of the  $U_{\text{eff}}$  parameter. Besides, the lattice constants obtained in GGA calculations are obviously too small in comparison with corresponding experimental results, for both  $\text{US}_3$  and  $\text{USe}_3$ . For  $\text{US}_3$ , the value of  $U_{\text{eff}}$  has to be as large as 6 eV to get reasonable lattice constants compared with experimental results. Differently, a  $U_{\text{eff}}$  value of 4 eV is enough to get reasonable lattice constants for  $\text{USe}_3$ , and changing  $U_{\text{eff}}$  from 4 to 6 eV has negligible effects on the obtained lattice constants.

Besides of the prominent changes in the atomic structure parameters, the most dramatic improvement brought by the GGA+ $U$  formalism when compared to the GGA results is in the description of electronic structure properties. For this, we have investigated the band structures in AFM phases for  $\text{US}_3$  and  $\text{USe}_3$  aiming at revealing the fundamental influences of considering the on-site Coulomb interaction. Figures 2(a) and 2(b) show the obtained local density of states (LDOS) for the S1, S3, and U atoms in  $\text{US}_3$ , and Se1, Se3, and U atoms in  $\text{USe}_3$  respectively. Without accounting for the on-site Coulomb repulsion, one can see that the GGA calculations predict an incorrect metallic ground state by nonzero occupation of uranium electrons at the Fermi energy ( $E_f$ ). When switching on the  $U_{\text{eff}}$  parameter, as shown both in Figs. 2(a) and 2(b), the uranium electronic states in  $\text{US}_3$  and  $\text{USe}_3$  begin to split at  $E_f$  and tend to form two peaks with the gap of  $\Delta E$ . The amplitude of this gap increases with increasing  $U_{\text{eff}}$ . Previous electric resistivity measurements pointed out that  $\text{USe}_3$  did not conduct at room temperatures<sup>50</sup>, thus a band gap at  $E_f$  should be contained in its electronic structure. We can see from Fig. 2(b) that an energy band gap appears only when  $U_{\text{eff}}$  is larger than or equal to 4 eV for  $\text{USe}_3$ . For  $\text{US}_3$ , the value of  $U_{\text{eff}}$  has to be enlarged to 6 eV to open the band gap at the Fermi energy. These results also imply that the electron correlation strength might be different in  $\text{US}_3$  and  $\text{USe}_3$ . From the last figure in Figs. 2(a) and 2(b), we can see that the sulphur (selenium) and uranium electronic states overlap with each other and contribute equally to the valence band maximum (VBM) of  $\text{US}_3$  ( $\text{USe}_3$ ), while the conduction band minimum (CBM) is composed of uranium electronic states. The orbital mixing between sulphur (selenium) and uranium electronic states below the Fermi energy indicates that there are covalent interactions between the sulphur (selenium) and

uranium atoms in  $\text{US}_3$  ( $\text{USe}_3$ ).

To further analyze the orbital-resolved electronic structures, we calculate the projected density of states (PDOS) for the  $X-np$  ( $n=3$  ( $X=\text{S}$ ) or  $4$  ( $X=\text{Se}$ )),  $\text{U-}5f$  and  $\text{U-}6p$  electronic states in  $\text{UX}_3$ . Figures 3(a)-3(d) show the obtained PDOS for  $\text{US}_3$  in different calculations, while the corresponding PDOS results for  $\text{USe}_3$  are shown in Figs. 3(e)-3(h). The value of  $U_{\text{eff}}$  is chosen to be 6 eV in all GGA+ $U$  and GGA+ $U$ +SOC calculations. One can see that without considering the electron correlation effect,  $\text{US}_3$  and  $\text{USe}_3$  are both wrongly predicted as metallic materials, which contradicts with experimental results. After adding the  $U$  parameter to describe the strong on-site energy of  $\text{U-}5f$  electrons, the energy gaps are opened for  $\text{US}_3$  and  $\text{USe}_3$ . We can see from Figs. 3(d) and 3(h) that further considering SOC has little influences on the electronic states around the Fermi energy. For both  $\text{US}_3$  and  $\text{USe}_3$ , the SOC effect lies in the deep energy level, causing an energy splitting of the  $\text{U-}6p$  states. From the PDOS results, we can also see clear difference between the  $\text{X1-}$  and  $\text{X3-}np$  ( $n=3$  ( $X=\text{S}$ ) or  $4$  ( $X=\text{Se}$ )) electronic states. The PDOS for the electronic states of the  $\text{X2}$  atom is very similar to that of the  $\text{X1}$  atom and thus is not shown here. The different electronic state distribution of the  $\text{X1(X2)}$  and  $\text{X3}$  atoms proves the theory of considering  $\text{UX}_3$  as  $\text{UX(X}_2\text{)}$ , and indicates the strong covalent bondings between the  $\text{X1}$  and  $\text{X2}$  atoms.

To analyze more carefully the SOC effects in  $\text{US}_3$  and  $\text{USe}_3$ , we recalculate the electronic structures of them with higher resolutions, with the reduced Gaussian smearing width of only 0.02 eV and a PDOS resolution of 0.01 eV. Figures 4(a) and 4(b) show the obtained PDOS results for uranium  $5f$  electrons of  $\text{US}_3$  and  $\text{USe}_3$ , by using the GGA method, while Figs. 5(a) and 5(b) show the obtained energy band structures of  $\text{US}_3$  and  $\text{USe}_3$  by using the GGA+ $U$  method, respectively. All the GGA+SOC and GGA+ $U$ +SOC calculations are noncollinear, with both SOC and orbital polarizations considered. And the results before and after considering the SOC effects are shown in solid and dotted lines respectively. From the PDOS results obtained by using the GGA method, we can see that pure inclusion of SOC to the GGA method does not lead to energy band gaps for  $\text{US}_3$  and  $\text{USe}_3$ . This discovery is different from the situation of  $\text{CoO}$ , where SOC can solely open a band gap<sup>51</sup>.

From the band structures of  $\text{US}_3$  shown in Fig. 5(a), we can see that both the lowest unoccupied conduction and highest occupied valence bands distribute along the  $\Gamma\text{-Z}$  direction. For the lowest conduction band, the SOC effect causes an energy downshift of 0.05 eV along the  $\Gamma\text{-Z}$  direction. Contrarily for its highest valence band, the SOC effect causes an energy

upshift of 0.03 eV at the  $\Gamma$  point and an upshift of 0.07 eV at the Z point. As a result, the energy band gap of  $\text{US}_3$  changes from indirect ( $\Gamma \rightarrow \text{Z}$ ) into direct type ( $\text{Z} \rightarrow \text{Z}$ ) after considering the SOC effect, and the gap value reduces from 1.59 to be 1.48 eV. Different from  $\text{US}_3$ , the lowest conduction and highest valence bands of  $\text{USe}_3$  distributes along the  $\text{K}_1\text{-B}$  and  $\text{B-}\Gamma\text{-Y}$  directions respectively. For the lowest conduction band along the  $\text{K}_1\text{-B}$  direction, the SOC effect causes an energy downshift of 0.04 eV at the  $\text{K}_1$  point and a downshift of 0.02 eV at the B point. Correspondingly the CBM of  $\text{USe}_3$  moves from B to the  $\text{K}_1$  point. However, since the VBM of  $\text{USe}_3$  is at some point along the  $\text{B-}\Gamma\text{-Y}$  direction instead of at any high-symmetry  $k$  points, the SOC effect does not change the indirect band gap type. Overall the band gap of  $\text{USe}_3$  changes from 1.30 to be 1.23 eV after considering the SOC effect. Our studies reveal that the energy band gap of  $\text{USe}_3$  is smaller than that of  $\text{US}_3$ .

After systematically presenting the electronic structure results for  $\text{US}_3$  and  $\text{USe}_3$ , we now turn to their mechanical properties. The elastic constants are obtained by solving the eigenvalues of their Hessian matrix, which is calculated based on the Hooke's law and small position changes on independent S, Se and U atoms. The obtained elastic constants of  $\text{US}_3$  and  $\text{USe}_3$  in different calculations by using the GGA and GGA+ $U$  methods are both listed in Table III. We can see that the elastic constants calculated by using the GGA formalism for  $\text{US}_3$  and  $\text{USe}_3$  do not satisfy the stability criteria<sup>52,53</sup> for monoclinic structures that the  $C_{11}$ ,  $C_{22}$ ,  $C_{33}$ ,  $C_{44}$ ,  $C_{55}$ ,  $C_{66}$  should be all positive. This result further proves that conventional GGA formalism fails for describing the uranium trichalcogenides. Contrarily, the calculated elastic constants by using the GGA+ $U$  method for both  $\text{US}_3$  and  $\text{USe}_3$  satisfy the above stability criteria, as well as the other six criteria for monoclinic structures<sup>52,53</sup>, proving the stable existence of  $\text{US}_3$  and  $\text{USe}_3$ , and their strong electron correlation effects.

Based on the elastic constants of  $\text{US}_3$  and  $\text{USe}_3$ , we further calculate the Voigt and Reuss bounds on their bulk ( $B_V$ ,  $B_R$ ) and shear moduli ( $G_V$ ,  $G_R$ )<sup>54</sup>. And the bulk and shear moduli of  $\text{US}_3$  and  $\text{USe}_3$  can be estimated by  $B=(B_V+B_R)/2$ , and  $G=(G_V+G_R)/2$ . And the Poisson's ratios can be calculated by  $\nu=(3B-2G)/(6B+2G)$ . The obtained mechanical properties for  $\text{US}_3$  and  $\text{USe}_3$  are all listed in Table IV. We can see that the Voigt and Reuss bounds obviously differ from each other for bulk and shear moduli. This result reflects the structural anisotropy of  $\text{US}_3$  and  $\text{USe}_3$ . Besides, the bulk and shear moduli are both found to be larger for  $\text{US}_3$  than for  $\text{USe}_3$ . The Poisson's ratio is calculated to be 0.19 and 0.22 for  $\text{US}_3$  and  $\text{USe}_3$  respectively.

Until now, there are no experimental reports on the mechanical properties of  $\text{US}_3$  or  $\text{USe}_3$ . Hence our theoretical values can be used as references for further investigations or industrial applications of them. At another side, the Raman properties of the  $\text{MX}_3$  group materials have been systematically studied for a long time, and some of the characteristic peaks of  $\text{US}_3$  and  $\text{USe}_3$  were successfully observed in experiments<sup>31</sup>. Therefore, here we further calculate the Raman properties of  $\text{US}_3$  and  $\text{USe}_3$ . According to group theory and the symmetry of them, both  $\text{US}_3$  and  $\text{USe}_3$  are predicted to have 12 Raman-active vibrational modes<sup>31,55</sup>: 8  $A_g$  and 4  $B_g$  modes respectively. The symbols  $A_g$  and  $B_g$  represent for two different vibration symmetries respectively: vibrations inside and out of the mirror plane. Specifically,  $A_g$  corresponds to the vibrations where  $dy$  is always 0 while  $B_g$  corresponds to the vibrations where  $dy$  is not 0.

Our Raman results of  $\text{US}_3$  and  $\text{USe}_3$  are obtained by symmetry analysis based on the vibrational modes calculated within the GGA+ $U$  method, where SOC effects are considered. Figures 6(a) and 6(b) show our determined Raman frequencies for  $\text{US}_3$  and  $\text{USe}_3$  respectively, together with the experimental results by G. Nouvel *et al.*<sup>31</sup>. One can see that by using the GGA formalism for both  $\text{US}_3$  and  $\text{USe}_3$ , the Raman frequencies are totally confused compared with the experimental results. At another side, the GGA+ $U$  results on the Raman frequencies are clearly reasonable in two obvious aspects: i) there exist a highest single Raman frequency for both  $\text{US}_3$  and  $\text{USe}_3$ , corresponding to the molecular-like  $X_2$  mode vibrations; ii) the highest Raman frequency of  $\text{US}_3$  is much larger than that of  $\text{USe}_3$ , indicating that the S-S interaction is stronger than Se-Se. When comparing all the Raman frequencies, there seems to be a frequency shift of about  $25\sim 35\text{ cm}^{-1}$  between our GGA+ $U$  and the experimental results.

#### IV. CONCLUSION

By using the GGA and GGA+ $U$  methods, we have systematically studied the electronic, mechanical, and Raman properties of  $\text{US}_3$  and  $\text{USe}_3$ , aiming to reveal the underlying electron correlation and SOC effects. By comparing the calculated lattice constants of  $\text{US}_3$  and  $\text{USe}_3$  with corresponding experimental results, and monitoring their electronic structures with different  $U_{\text{eff}}$  parameters, we conclude that a  $U_{\text{eff}}$  value of 6 eV is needed to get reasonable lattice constants, and the right insulating properties for both  $\text{US}_3$  and  $\text{USe}_3$ . After



considering SOC effects, the deep U-6*p* band will be split into two separate energy bands in both US<sub>3</sub> and USe<sub>3</sub>. The SOC effects also changes the energy band shapes around the Fermi energies and lead to the fact that US<sub>3</sub> is a direct band gap while USe<sub>3</sub> is an indirect band gap insulator. Because of the SOC effects, the energy band gaps of US<sub>3</sub> and USe<sub>3</sub> reduce by 0.11 and 0.07 eV respectively. Based on the obtained antiferromagnetic ground states of US<sub>3</sub> and USe<sub>3</sub>, we then systematically give out their electrical, mechanical, and Raman properties. The VBM and CBM of US<sub>3</sub> (USe<sub>3</sub>) are found to be contributed by 3*p*-5*f* (4*p*-5*f*) hybrid and 5*f* (5*f*) electronic states respectively. The elastic constants of US<sub>3</sub> and USe<sub>3</sub> are found to satisfy the stability criteria, and their Poisson's ratios are calculated to be 0.19 and 0.22 respectively. For the Raman properties, we theoretically repeat the two important experimental observations that the S-S or Se-Se dimer vibrations have the largest frequencies in US<sub>3</sub> and USe<sub>3</sub>, and the frequency of the S-S dimer vibration is larger than that of the Se-Se dimer vibration.

## V. ACKNOWLEDGEMENT

This work was supported by the National Natural Science Foundation of China under Grants No. 10904004 and No. 90921003 and Foundations for Development of Science and Technology of China Academy of Engineering Physics under Grants No. 2011B0301060, No. 2011A0301016, and No. 2008A0301013.

---

\* Corresponding author. zhang\_ping@iapcm.ac.cn

<sup>1</sup> S. Y. Savrasov, G. Kotliar, and E. Abrahams, Nature **410**, 793 (2001).

<sup>2</sup> R. C. Albers, Nature **410**, 759 (2001).

<sup>3</sup> S. S. Hecker, Metall. Mater. Trans. A **35**, 2207 (2004).

<sup>4</sup> K. T. Moore, G. van der Laan, R. G. Haire, M. A. Wall, and A. J. Schwartz, Phys. Rev. B **73**, 033109 (2006).

<sup>5</sup> I. D. Prodan, G. E. Scuseria, and R. L. Martin. Phys. Rev. B **73**, 045104 (2006).

<sup>6</sup> I. D. Prodan, G. E. Scuseria, and R. L. Martin. Phys. Rev. B **76**, 033101 (2007).

<sup>7</sup> S. L. Dudarev, D. N. Manh, and A. P. Sutton, Philos. Mag. B **75**, 613 (1997).

- <sup>8</sup> S. L. Dudarev, G. A. Botton, S. Y. Savrasov, C. J. Humphreys, and A. P. Sutton, Phys. Rev. B **57**, 1505 (1998).
- <sup>9</sup> S. L. Dudarev, M. R. Castell, G. A. Botton, S. Y. Savrasov, C. Muggelberg, G. A. D. Briggs, A. P. Sutton, and D. T. Goddard, Micron **31**, 363 (2000).
- <sup>10</sup> B. Sun, P. Zhang, and X. G. Zhao, J. Chem. Phys. **128**, 084705 (2008).
- <sup>11</sup> B. Sun and Z. Ping, Chin. Phys. B **17**, 1364 (2008).
- <sup>12</sup> H. Shi, M. F. Chu, and P. Zhang, J. Nucl. Mater. **400**, 151 (2010).
- <sup>13</sup> B. T. Wang, H. L. Shi, W. D. Li, and P. Zhang, Phys. Rev. B **81**, 045119 (2010).
- <sup>14</sup> P. Zhang, B. T. Wang, and X. G. Zhao, Phys. Rev. B **82**, 144110 (2010).
- <sup>15</sup> S. Kern, R. A. Robinson, H. Nakotte, G. H. Lander, B. Cort, P. Watson, and F. A. Vigil, Phys. Rev. B **59**, 104 (1999).
- <sup>16</sup> L. Petit, A. Svane, Z. Szotek, and W. M. Temmerman, Science **301**, 498 (2003).
- <sup>17</sup> L. Petit, A. Svane, Z. Szotek, W. M. Temmerman, and G. M. Stocks, Phys. Rev. B **81**, 045108 (2010).
- <sup>18</sup> S. B. Wilkins, R. Caciuffo, C. Detlefs, J. Rebizant, E. Colineau, F. Wastin, and G. H. Lander, Phys. Rev. B **73**, 060406 (2006).
- <sup>19</sup> Q. Yin and S. Y. Savrasov, Phys. Rev. Lett. **100**, 225504 (2008).
- <sup>20</sup> G. Jomard, B. Amadon, F. Bottin, and M. Torrent, Phys. Rev. B **78**, 075125 (2008).
- <sup>21</sup> D. A. Andersson, J. Lezama, B. P. Uberuaga, C. Deo, and S. D. Conradson, Phys. Rev. B **79**, 024110 (2009).
- <sup>22</sup> P. Santini, S. Carretta, G. Amoretti, R. Caciuffo, N. Magnani, and G. H. Lander, Rev. Mod. Phys. **81**, 807 (2009).
- <sup>23</sup> M. Sanati, R. C. Albers, T. Lookman, and A. Saxena, Phys. Rev. B **84**, 014116 (2011).
- <sup>24</sup> B. Dorado, B. Amadon, M. Freyss, and M. Bertolus, Phys. Rev. B **79**, 235125 (2009).
- <sup>25</sup> B. Dorado, G. Jomard, M. Freyss, and M. Bertolus, Phys. Rev. B **82**, 035114 (2010).
- <sup>26</sup> H. Nakamura, M. Machida, and M. Kato, Phys. Rev. B **82**, 155131 (2010).
- <sup>27</sup> B. Meredig, A. Thompson, H. A. Hansen, C. Wolverton, and A. van de Walle, Phys. Rev. B **82**, 195128 (2010).
- <sup>28</sup> H. Y. Geng, Y. Chen, Y. Kaneta, M. Kinoshita, and Q. Wu, Phys. Rev. B **82**, 094106 (2010).
- <sup>29</sup> H. Yasuoka, G. Koutroulakis, H. Chudo, S. Richmond, D. K. Veirs, A. I. Smith, E. D. Bauer, J. D. Thompson, G. D. Jarvinen, D. L. Clark, Science **336**, 901 (2012).

- <sup>30</sup> M. E. Manley, J. R. Jeffries, A. H. Said, C. A. Marianetti, H. Cynn, B. M. Leu, and M. A. Wall, Phys. Rev. B **85**, 132301 (2012).
- <sup>31</sup> G. Nouvel, A. Zwick, M. A. Renucci, D. J. Lockwood, and H. Noël, J. Phys. C: Solid State Phys. **20**, 1881 (1987).
- <sup>32</sup> J. Schäfer, M. Sing, R. Claessen, E. Rotenberg, X. J. Zhou, R. E. Thorne, and S. D. Kevan, Phys. Rev. Lett. **91**, 066401 (2003).
- <sup>33</sup> A. Perucchi, L. Degiorgi, and R. E. Thorne, Phys. Rev. B **69**, 195114 (2004).
- <sup>34</sup> A. Perucchi, L. Degiorgi, and H. Berger, Eur. Phys. J. B **48**, 489 (2004).
- <sup>35</sup> T. Yokoya, T. Kiss, A. Chainani, S. Shin, and K. Yamaya, Phys. Rev. B **71**, 140504(R) (2005).
- <sup>36</sup> D. Pacilé, M. Papagno, M. Lavagnini, H. Berger, L. Degiorgi, and M. Grioni, Phys. Rev. B **76**, 155406 (2007).
- <sup>37</sup> G. Kresse and J. Furthmüller, Phys. Rev. B **54**, 11169 (1996) and references therein.
- <sup>38</sup> J. P. Perdew, K. Burke, and M. Ernzerhof, Phys. Rev. Lett. **77**, 3865 (1996).
- <sup>39</sup> J. P. Perdew, K. Burke, and M. Ernzerhof, Phys. Rev. Lett. **78**, 1396 (1997).
- <sup>40</sup> P. E. Blöchl, Phys. Rev. B **50**, 17953 (1994).
- <sup>41</sup> H. J. Monkhorst and J. D. Pack, Phys. Rev. B **13**, 5188 (1976).
- <sup>42</sup> A. Kotani and T. Yamazaki, Prog. Theor. Phys. Supp. **108**, 117 (1992).
- <sup>43</sup> W. Trzebiatowski and W. Suski, Bull. Acad. Pol. Sci. Sér. Sci. Chim. **9**, 277 (1961).
- <sup>44</sup> W. Suski, Bull. Acad. Pol. Sci. Sér. Sci. Chim. **24**, 75 (1976).
- <sup>45</sup> M. Baran, H. Szymczak, B. Janus, and W. Suski, Solid State Commun. **48**, 569 (1983).
- <sup>46</sup> H. Noël, J. Less-Common Met. **121**, 265 (1986).
- <sup>47</sup> F. Gronvold, H. Haraldsen, T. T. Moe, and T. Tufte, J. Inorg. Nucl. Chem. **30**, 2117 (1968).
- <sup>48</sup> A. B. Salem, A. Meerschaut, and J. Rouxel, C. R. Acad. Sci. Paris II **299**, 617 (1984).
- <sup>49</sup> B. T. Wang, H. L. Shi, W. D. Li, and P. Zhang, Phys. Rev. B **81**, 045119 (2010).
- <sup>50</sup> L. Shlyk, R. Troć, and D. Kaczorowski, J. Magn. Magn. Mater. **140-144**, 1435 (1995).
- <sup>51</sup> M. R. Norman, Phys. Rev. Lett. **64**, 1162 (1990).
- <sup>52</sup> J. F. Nye, *Physical Properties of Crystals* (Oxford University Press, Oxford, 1985).
- <sup>53</sup> Z. J. Wu, E. J. Zhao, H. P. Xiang, X. F. Hao, X. J. Liu, and J. Meng, Phys. Rev. B **76**, 054115 (2007).
- <sup>54</sup> See Supplementary Material Document No. \_\_\_\_\_ for computational details of the Voigt and Reuss bounds on bulk ( $B_V$ ,  $B_R$ ) and shear moduli ( $G_V$ ,  $G_R$ ) of  $\text{US}_3$  and  $\text{USe}_3$ .

<sup>55</sup> A. Zwick and M. A. Renucci, Phys. Status Solidi B **96**, 757 (1979).

TABLE I: Electronic energies per unit cell of  $\text{US}_3$  and  $\text{USe}_3$  in the nonmagnetic (NM), ferromagnetic (FM), and antioferromagnetic (AFM) states by using different calculation methods. All values are in units of eV.

Methods	$\text{US}_3$			$\text{USe}_3$		
	NM	FM	AFM	NM	FM	AFM
GGA	-55.33	-55.55	-55.47	-50.48	-50.87	-50.79
GGA+ $U$ ( $U_{\text{eff}}=1$ eV)	-53.30	-53.82	-53.78	-48.46	-49.30	-49.31
GGA+ $U$ ( $U_{\text{eff}}=2$ eV)	-51.34	-52.50	-52.24	-46.57	-48.14	-48.17
GGA+ $U$ ( $U_{\text{eff}}=3$ eV)	-49.68	-51.53	-51.53	-45.07	-47.72	-47.72
GGA+ $U$ ( $U_{\text{eff}}=4$ eV)	-48.42	-50.85	-50.85	-44.50	-47.26	-47.35
GGA+ $U$ ( $U_{\text{eff}}=5$ eV)	-46.55	-50.74	-50.74	-43.95	-46.79	-47.26
GGA+ $U$ ( $U_{\text{eff}}=6$ eV)	-48.39	-51.68	-51.69	-43.48	-46.52	-46.85

TABLE II: Lattice constants of  $\text{US}_3$  and  $\text{USe}_3$  obtained by using different methods. All values are in units of  $\text{\AA}$ .

Methods	$\text{US}_3$			$\text{USe}_3$		
	$a$	$b$	$c$	$a$	$b$	$c$
GGA	5.11	3.83	9.25	5.50	3.99	10.22
GGA+ $U$ ( $U_{\text{eff}}=1$ eV)	5.12	3.82	9.26	5.52	3.95	10.30
GGA+ $U$ ( $U_{\text{eff}}=2$ eV)	5.13	3.82	9.28	5.52	3.94	10.42
GGA+ $U$ ( $U_{\text{eff}}=3$ eV)	5.09	3.74	9.61	5.50	3.87	10.98
GGA+ $U$ ( $U_{\text{eff}}=4$ eV)	5.09	3.75	9.65	5.71	4.02	10.90
GGA+ $U$ ( $U_{\text{eff}}=5$ eV)	5.06	3.82	9.61	5.73	4.04	10.52
GGA+ $U$ ( $U_{\text{eff}}=6$ eV)	5.44	3.92	9.76	5.73	4.04	10.60
Exp. <sup><i>a,b</i></sup>	5.37	3.96	9.94	5.65	4.06	10.47

<sup>*a*</sup>Reference 47

<sup>*b*</sup>Reference 48

TABLE III: Elastic constants of  $\text{US}_3$  and  $\text{USe}_3$  obtained in GGA and GGA+ $U$ +SOC calculations. The  $U_{\text{eff}}$  value is chosen to be 6 eV in both GGA+ $U$ +SOC calculations. All data are in units of GPa.

	$C_{11}$	$C_{22}$	$C_{33}$	$C_{44}$	$C_{55}$	$C_{66}$	$C_{12}$	$C_{13}$	$C_{23}$	$C_{45}$	$C_{16}$	$C_{26}$	$C_{36}$
$\text{US}_3$ (GGA)	-654	-80	-4132	452	-332	-273	-923	-2953	-1766	32	-511	-640	-522
$\text{US}_3$ (GGA+ $U$ +SOC)	963	1055	437	313	299	169	196	132	181	-6	-102	-55	-74
$\text{USe}_3$ (GGA)	946	583	-107	363	309	7	-37	-349	-65	3	171	24	198
$\text{USe}_3$ (GGA+ $U$ +SOC)	951	938	496	257	244	267	195	194	216	-13	-19	-20	-33

TABLE IV: Mechanical properties of  $\text{US}_3$  and  $\text{USe}_3$  including the bulk and shear moduli, their Voigt and Reuss bounds, and the Poisson's ratio calculated by using the GGA+ $U$  method. The  $U_{\text{eff}}$  value is chosen to be 6 eV. All moduli data are in units of GPa.

	$B_V$	$B_R$	$G_V$	$G_R$	$B$	$G$	$\nu$
$\text{US}_3$	386	299	286	245	342	266	0.19
$\text{USe}_3$	400	365	272	257	382	265	0.22



## List of captions

**Fig.1** (Color online). (a) The atomic structures of  $\text{MX}_3$ , where blue and dark green balls representing for metal (M) and chalcogen (X) atoms respectively. The monoclinic lattices are depicted by the dashed lines. (b) Depiction of the Brillouin Zone for the monoclinic  $\text{MX}_3$  lattice.

**Fig.2** (Color online). The local density of states (LDOS) for the S1, S3, and U atoms in  $\text{US}_3$  (a) and Se1, Se2, and U atoms in  $\text{USe}_3$  (b) by using the GGA and GGA+ $U$  methods with  $U_{\text{eff}}$  ranging from 1 to 6 eV. The S1 (Se1) and S3 (Se3) atoms correspond to X1 and X3 atoms depicted in Fig. 1(a). The Fermi energies are denoted by dashed lines.

**Fig.3** (Color online). (a)-(d) The projected density of states (PDOS) for the  $3p$  electronic states of S1 and S3 atoms, and  $5f$ ,  $6p$  electronic states of the U atom in  $\text{US}_3$ . (e)-(h) The PDOS for the  $4p$  electronic states of Se1 and Se3 atoms, and  $5f$ ,  $6p$  electronic states of the U atom in  $\text{USe}_3$ . The S1 (Se1) and S3 (Se3) atoms correspond to X1 and X3 atoms depicted in Fig. 1(a). The Fermi energies are denoted by dashed lines. The values of  $U_{\text{eff}}$  are chosen to be 6 eV in all GGA+ $U$  and GGA+ $U$ +SOC calculations.

**Fig.4** (Color online). The projected density of states for the uranium  $5f$  electronic states in  $\text{US}_3$  (a) and  $\text{USe}_3$  (b), by using the GGA method. The Fermi energies are set to be zero and denoted by dashed lines. The results before and after considering the spin-orbit coupling effects are shown in red solid and blue dotted lines respectively.

**Fig.5** (Color online). The electronic energy band structures for  $\text{US}_3$  (a) and  $\text{USe}_3$  (b) by using the GGA+ $U$  method. The values of  $U_{\text{eff}}$  are chosen to be 6 eV. The Fermi energy and different  $k$ -points are denoted by the dashed lines. The results before and after considering the spin-orbit coupling effects are shown in solid and dotted lines respectively.

**Fig.6** (Color online). The calculated frequencies at the  $\Gamma$  point for Raman-active vibrational modes of  $\text{US}_3$  (a) and  $\text{USe}_3$  (b) by using the GGA and GGA+ $U$  methods, together with the experimental results listed in Ref. 31. The values of  $U_{\text{eff}}$  are chosen to be

6 eV. The symmetry for each vibration mode are also presented.

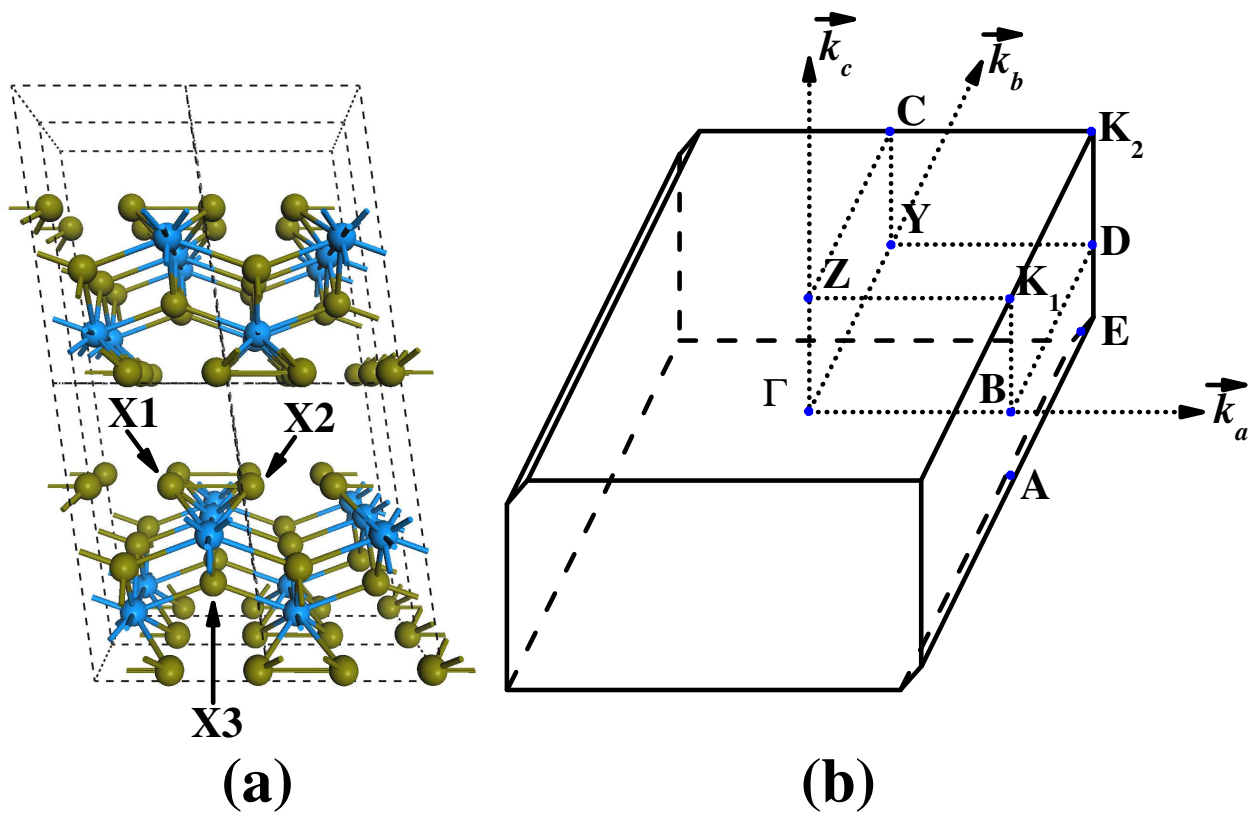


FIG. 1:

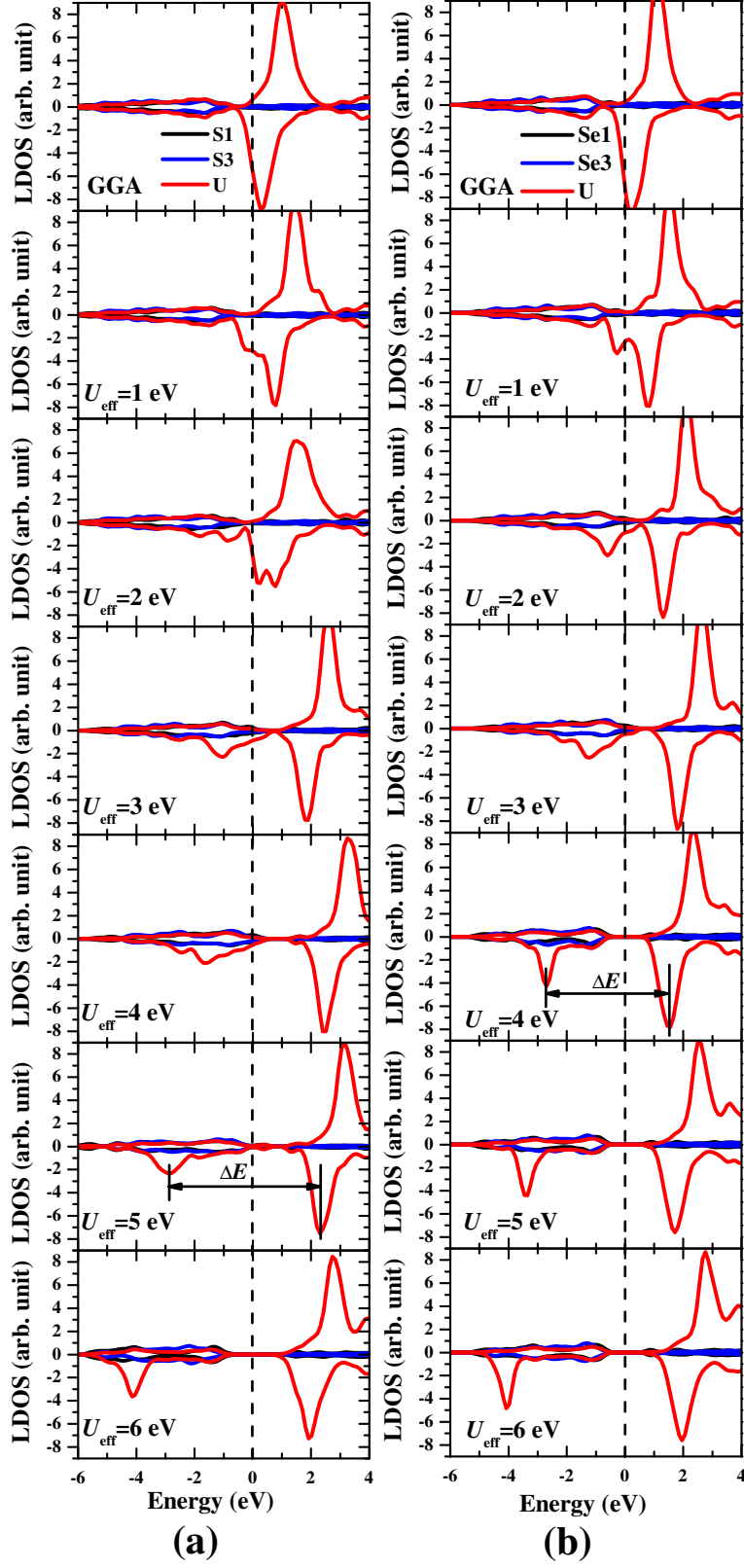


FIG. 2:

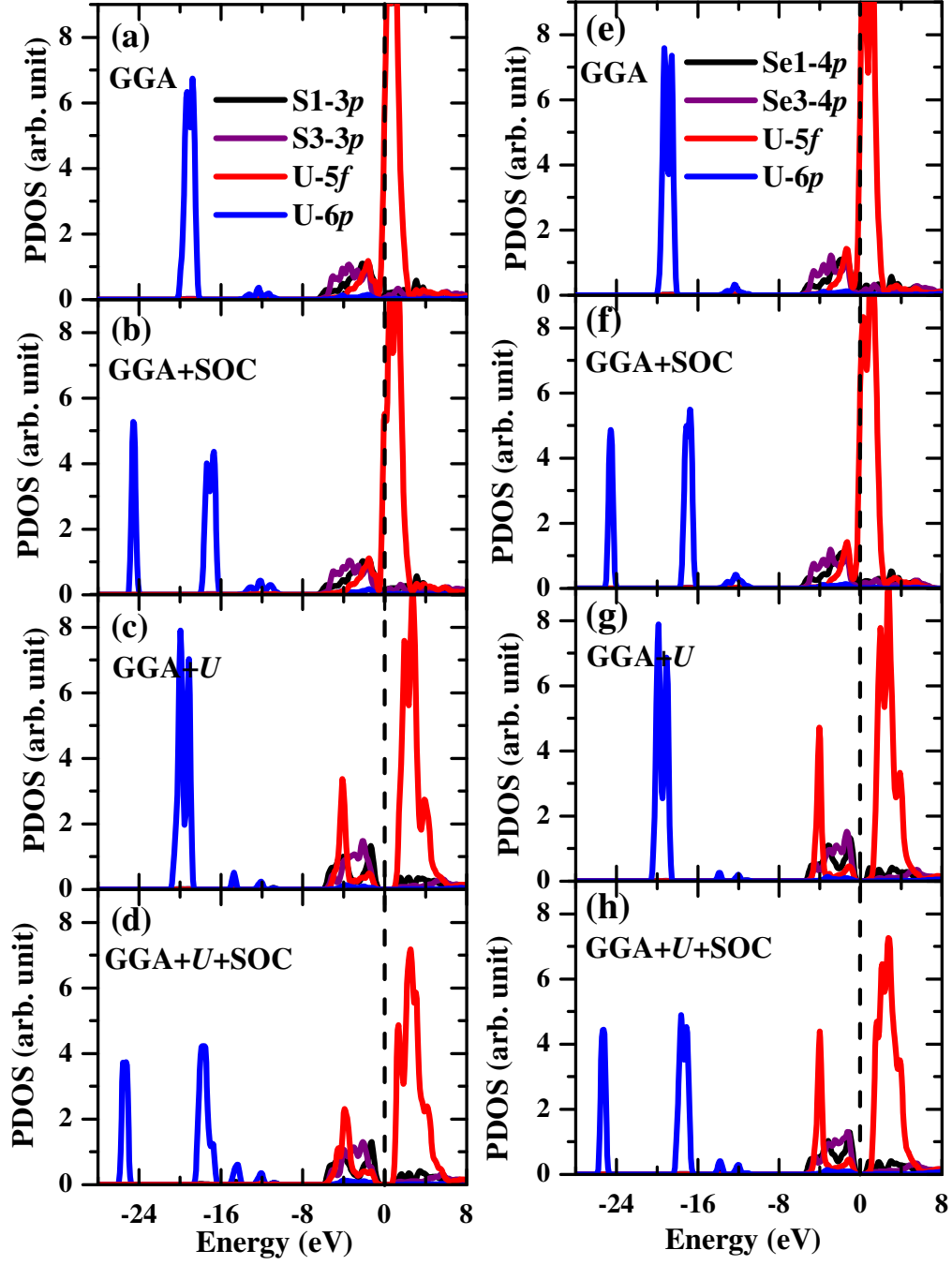


FIG. 3:

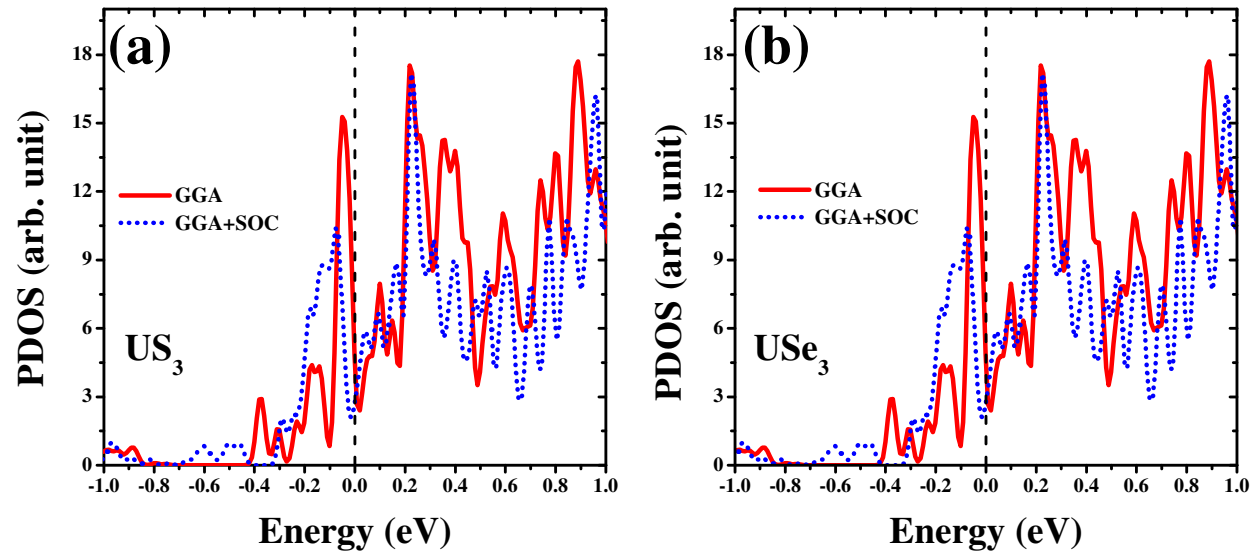


FIG. 4:

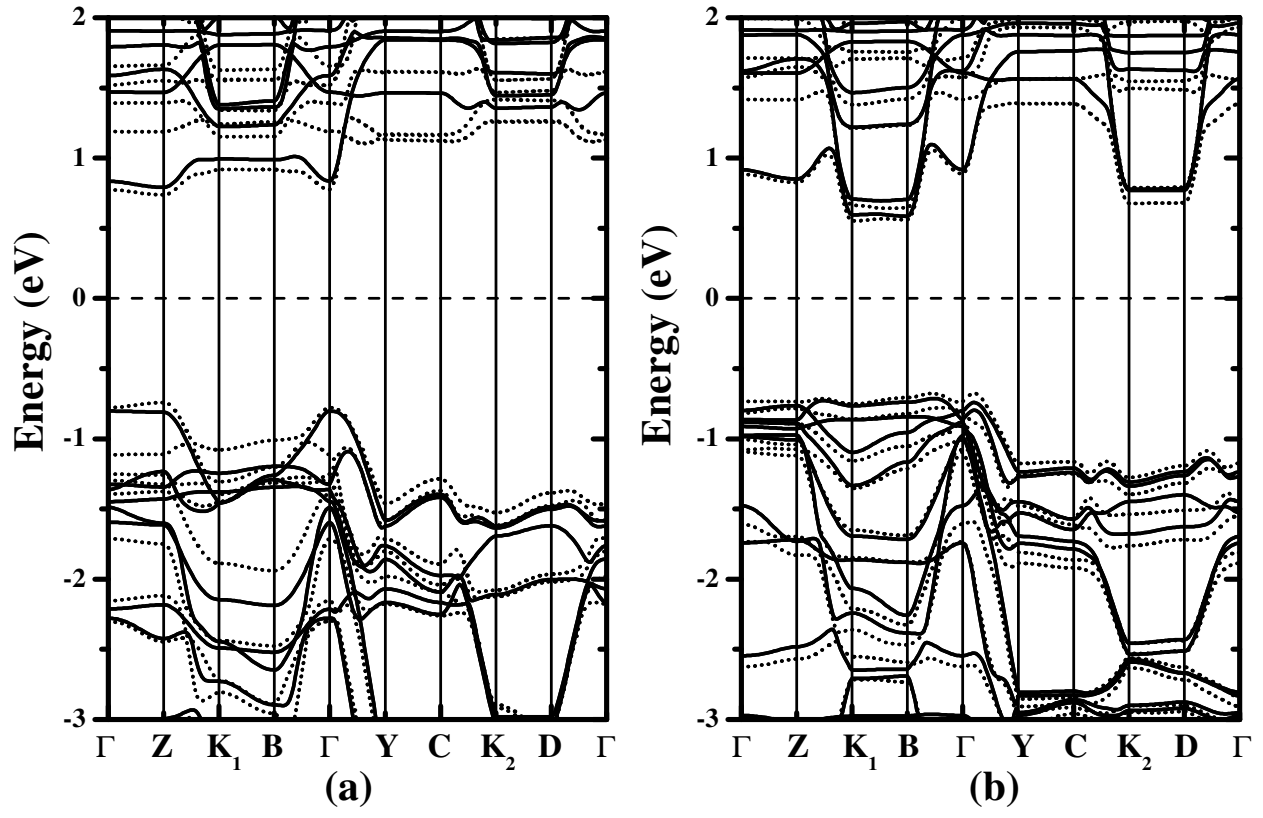


FIG. 5:

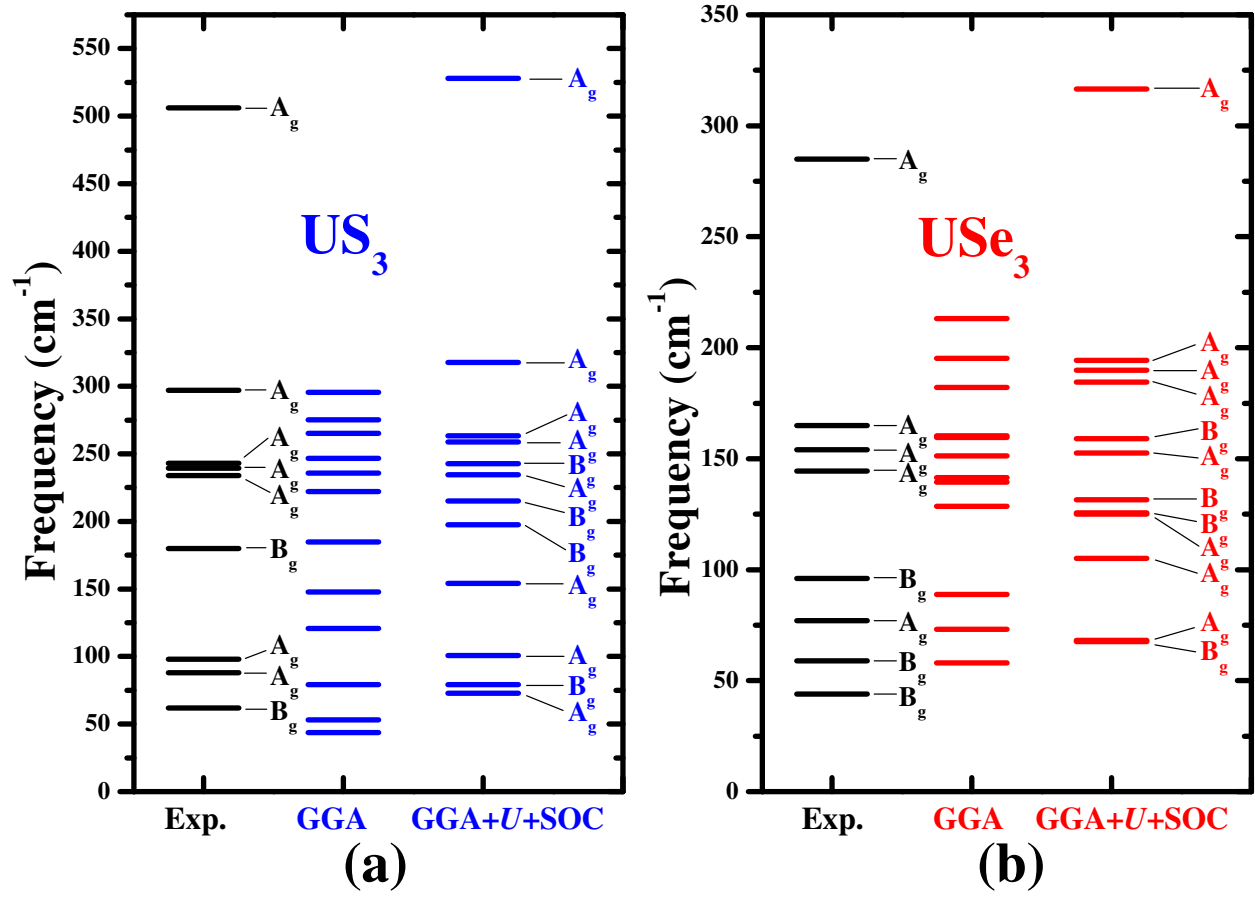


FIG. 6:



